Electron spin resonance of excited states of the H3 and H4 centres in irradiated type Ia diamonds



1995 J. Phys.: Condens. Matter 7 5901

(http://iopscience.iop.org/0953-8984/7/29/017)

J. Phys.: Condens. Matter 7 (1995) 5901–5911. Printed in the UK

# Electron spin resonance of excited states of the H3 and H4 centres in irradiated type Ia diamonds

J A van Wyk† and G S Woods‡

† Department of Physics, University of the Witwatersrand, Wits 2050, Johannesburg, South Africa

‡ CSO Valuations AG, 17 Charterhouse Street, London EC1N 6RA, UK

Received 13 February 1995, in final form 24 April 1995

**Abstract.** Electron spin resonance spectra, denoted W26 and W25, observed in type Ia diamonds showing the H3 and H4 optical absorptions, respectively, are shown to be due to excited states of the defects responsible for these absorptions. Zero-field and hyperfine parameters have been determined and are presented in this paper. The models proposed earlier by Loubser and van Wyk for the H4/W25 defect, and thus by extension also for the B nitrogen aggregate, are confirmed by the present work. The ESR results also support the the model proposed by Davies for the H3 centre.

## 1. Introduction

The H3 and H4 optical bands, with zero-phonon lines at 503.2 nm (2.463 eV) and 496.0 nm (2.499 eV), respectively, are well known vibronic bands in type Ia diamonds. Both are readily observed when laboratory-irradiated type Ia specimens are heated to above ≈550 °C, the temperature at which the vacancy in diamond becomes mobile. Type Ia diamonds quite generally contain two nitrogenous aggregates, namely A centres (involving two adjacent substitutional nitrogen atoms) and B centres (involving a small even number, greater than two, of nitrogen atoms). In irradiated and annealed specimens the ratio of the strengths of H3 and H4 is proportional to the ratio of the concentrations of the A and B aggregates, taken in this order (Davies and Summersgill 1973). It is thus generally accepted that the H3 and H4 centres are formed when a vacancy is trapped by an A or B aggregate, respectively. Polarized luminescence (Elliott *et al* 1958, Clark and Norris 1970) and uniaxial stress measurements (Runciman 1965, Davies *et al* 1976) have shown that H3 is due to transitions at a centre with rhombic I symmetry (Kaplyanskii 1964), with point group $C_{2v}$. The $C_2$ rotation axis is in an ⟨001⟩ direction and the mirror planes are {011}. Similar measurements (Clark and Norris 1970, de Sa and Davies 1977) have established that H4 is a dipolar transition at a centre with monoclinic I symmetry (Kaplyanskii 1964), with point group $C_{1h}$ and {011} the mirror plane.

None of the A, B, H3 and H4 defects is ordinarily paramagnetic. However, it has been reported briefly (van Wyk and Loubser 1980) that if certain diamonds containing H3 centres are illuminated with light of wavelength less than ≈500 nm a paramagnetic centre with either two or three unpaired electrons appears. The angular dependence of the ESR fine structure is close to being axially symmetric about ⟨011⟩. This centre was named W26. In other diamonds, in which H4 dominated, a similar ESR centre, called W25, was

0953-8984/95/295901+11$19.50  

observed under similar excitation conditions. The ESR spectra were again nearly axially symmetric about (011). However, the ESR centres were not observed in all diamonds that showed the H3 and/or H4 optical absorptions. A second precondition for the observation of W25 and W26 was that the (irradiated and annealed) specimens exhibited strong greenish luminescence under ultraviolet stimulation (an observation which will be discussed in more detail in section 4). The ESR lines of both centres are split by hyperfine interactions that vary in a complicated manner as as the crystal is rotated in the magnetic field.

The model proposed for the H3 centre (Davies 1976) involves the capture by the A aggregate of a vacancy (V) to yield, initially, the configuration N–N–V, with the instantaneous relaxation of a nitrogen atom into the vacancy to give the arrangement N–V–N. The properties and behaviour of W26 were reported by Loubser and van Wyk (1981) to be consistent with the latter configuration, and it was suggested that W26 and H3 were transitions at the same centre. The structure of the H3/W26 centre is shown in figure 1(a).

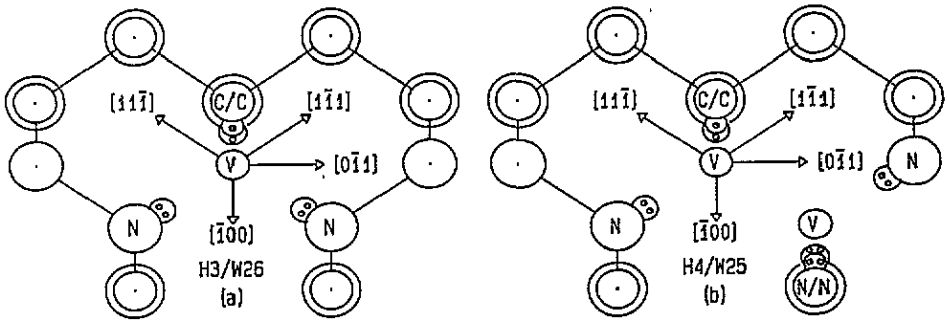


**Figure 1.** Models for the H3 and H4 centres projected on a {110} plane. The specific axis, labelled, will be referred to in the text. The single circles refer to atoms (or vacancies) in the plane of the paper, whereas the pairs of concentric circles refer to next planes of atoms, above and below the plane of the paper. The small circles on the labelled atoms show the electrons on the dangling bonds around the vacancy.

In order to understand the development of a model for the H4 centre, it is useful to consider first the structure of an optical defect called N3 (Clark *et al* 1956). This centre has an ESR analogue called P2 (Davies *et al* 1978, Loubser and van Wyk 1978). P2 (and thus N3) has been shown (van Wyk 1982, van Wyk and Loubser 1993) to comprise three adjacent substitutional nitrogen atoms in a {111} plane with a vacancy as common neighbour. We denote this by the shorthand notation $N_3$–V–C. Loubser and van Wyk (1981) noted that if the B centre consisted of four nitrogen atoms plus a vacancy in the configuration $N_3$–V–N (equivalent formally to an N3 centre with the carbon replaced by a nitrogen atom), and that if H4 resulted when a B centre captured an additional vacancy to give $N_3$–V–N–V, relaxing to $N_3$–V–V–N, then the latter configuration has properties consistent with both the luminescence and stress data for H4 and the ESR characteristics of W25. It was proposed that H4 and W25 were optical and ESR transitions, respectively, at one and the same centre. The proposed structure for the H4/W25 centre is shown in figure 1(b).

In the present paper we report more fully the analysis of the ESR spectra W25 and W26. We have also irradiated and isochronally annealed, at temperature intervals of 40 °C between 320 °C and 840 °C, diamonds that were carefully selected as to type by examination of

their infrared (IR) one-phonon absorption spectra, and examined the optical and ESR spectra after each anneal. This procedure has confirmed one to one correspondences between W26 and H3 on the one hand, and W25 and H4 on the other. The work thus places on a firmer footing the Loubser and van Wyk (1981) model for H4, and thus by extension for the B centre, and also offers further support for Davies' (1976) model for the H3 centre.

## 2. Experimental details

Two specimens of type IaA containing only A centres (OP1 and OP2), two of type IaB containing only B aggregates (A35 and CB7) and three of type IaA/B containing both aggregates (OP3, OP4 and OP5), were selected on the basis of their IR spectra. Representative IR spectra are shown in figure 2. In order to facilitate recognition of a specific crystal axis for the ESR measurements, the crystals were oriented using Laue photographs and a pair of parallel facets polished onto each, parallel, to within a few degrees, to {011}.

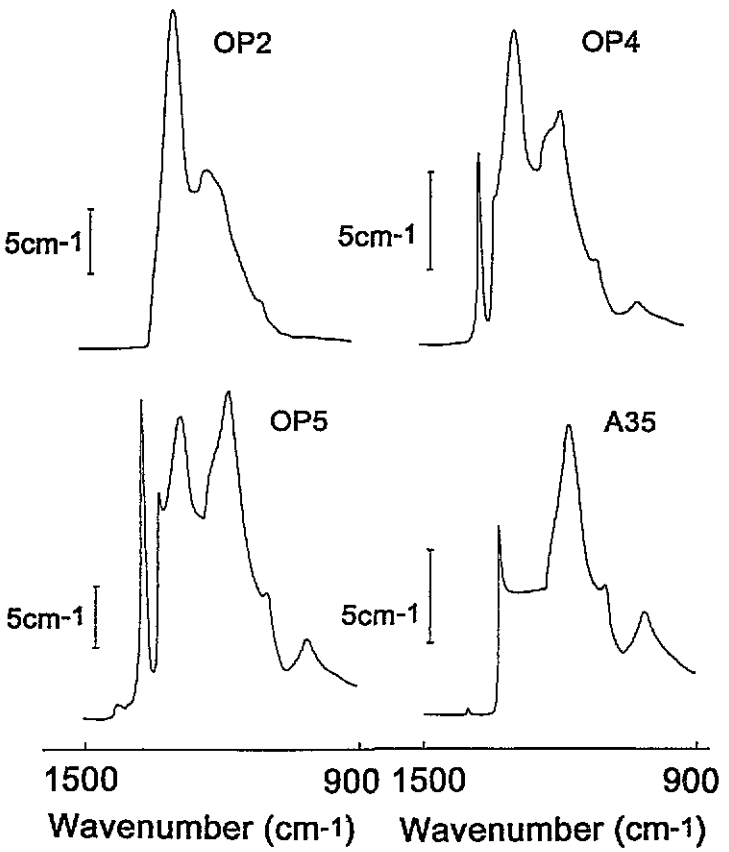


**Figure 2.** Infrared spectra of some of the diamonds selected on the basis of their IR absorptions.

The specimens were given a dose of $10^{18}$ electrons $cm^{-2}$. Anneals were of 10 minutes duration and were carried out with the specimens in a flow of nitrogen gas.

The ESR spectra were recorded at room temperature with a Varian E-line spectrometer. A high-pressure mercury source was employed for specimen illumination. Optical

spectra were recorded with the specimens at 77 K using a Perkin–Elmer model 330 spectrophotometer, and the IR spectra were taken at room temperature with a Perkin–Elmer PE580B spectrophotometer fitted with an 8× beam condenser.

## 3. Results

### *3.1. Analysis of the ESR spectra*

*3.1.1. Angular dependence of the fine structure.* The angular dependences of the spectra of both W25 and W26 are plotted as stars in figure 3. Clearly, both spectra are essentially axially symmetric about an ⟨011⟩ direction. For purposes of discussion we shall refer to this axis as the $z$ axis. The angular dependences of the spectra as the field is varied in the plane perpendicular to the $z$ axis, which will then be the $x$–$y$ plane, are represented by the line(s) starting at [100] and ending at $[0\bar{1}1]$ in figure 3. It is evident from this angular dependence that the tensors of the zero-field splitting ($D$ tensors) for both centres have a rhombic component. For W26 one of the principal axes of the $D$ tensor is obviously parallel to the twofold axis of the defect. The fact that this angular dependence splits for W25 shows that the tensor for this defect does not have a principal axis parallel to the [100] direction. This dependence in fact shows that one principal axis of the tensor is along a ⟨111⟩ direction.

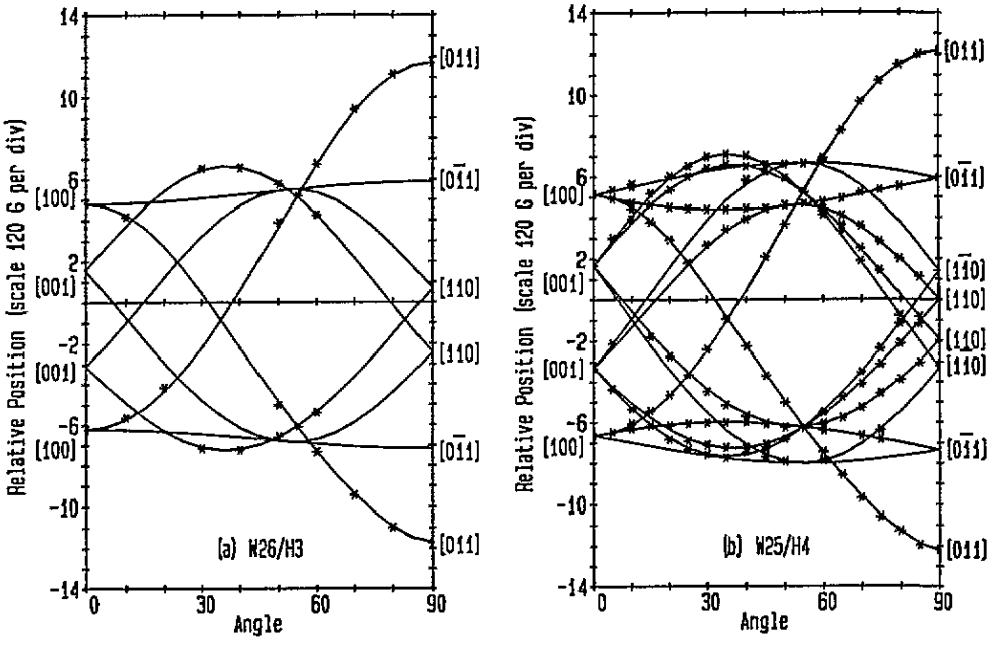


**Figure 3.** Angular dependence of (a) W26 and (b) W25 in the {110} planes. The stars represent the positions of experimental spectra. The solid lines represent positions calculated using the parameters in table 1. The labels of the directions in the figure apply if the plane in figure 1 is specifically the (011) plane. The uppermost and and third positions from the top, where the angle is ≈55° in (b), then correspond to $[11\bar{1}]$ and $[1\bar{1}1]$, respectively.

From the number of lines present we must have $S = 1$ or $S = \frac{3}{2}$. An $S = \frac{3}{2}$ spectrum would be distinguishable from an $S = 1$ spectrum by its having, in the $g = 2$ region, a third

**Table 1.** Zero-field splitting parameters for W25 and W26.

| Parameter | W25 | W26 |
|---|---|---|
| $g$ | 2.0027(4) | 2.0027(4) |
| $D_{xx}$ (MHz) | 1606(5) ∥ [$\bar{1}\bar{1}$1] | 1428(5) ∥ [0$\bar{1}$1] |
| $D_{zz}$ (MHz) | −2732(5) ∥ [011] | −2630(5) ∥ [011] |

line halfway between each pair of outer lines. Because of the quite general interference, in the $g = 2$ region, of intense spectra due to defects other than those of immediate interest, it was difficult to establish whether the third line is present. However, the models for W25 and W26 contain an even number of nitrogen atoms; if the defects are in their neutral charge states, the spin must be integer or zero. Furthermore, no ground state EPR has been observed for the defects. If $S = \frac{3}{2}$ for the defects, it ought to have been accompanied by an $S = \frac{1}{2}$ ground state. This led us to assume that $S = 1$. Further conclusive support for this assumption follows from the nature of the hyperfine structure, as will be discussed later.

The model in figure 1(a) for W26 suggests that one of the principal axes of the defect should be along the [100] direction. No ESR signals could be detected in the plane perpendicular to the $z$ axis of the defect (the plane of figure 1(a)). This means that the zero-field interaction does not provide direct proof that one axis of W25 is parallel to the twofold axis, but, as will be discussed later, the hyperfine interaction does provide such evidence.

The solid lines in figure 3 were calculated using the spin Hamiltonian

$$\mathcal{H} = g\beta \boldsymbol{H} \cdot \boldsymbol{S} + \boldsymbol{S} \cdot \boldsymbol{D} \cdot \boldsymbol{S} \tag{1}$$

where the symbols have their usual meanings. The parameters are given in table 1. In deriving these parameters it was assumed that the $x$ axis of the zero-field interaction is parallel to the principal axis along which the splitting is largest in the $x$–$y$ plane. More will be said in the next sections about the signs of the zero-field parameters.

*3.1.2. Hyperfine structure.* To describe the hyperfine spectra the following set of terms must be added to the spin Hamiltonian in section 3.1.1:

$$\boldsymbol{S} \cdot \boldsymbol{A}_i \cdot \boldsymbol{I}_i - \beta_N \boldsymbol{H} \cdot \boldsymbol{g}_{Ni} \cdot \boldsymbol{I}_i + \boldsymbol{I}_i \cdot \boldsymbol{P}_i \cdot \boldsymbol{I}_i \tag{2}$$

one set for each nitrogen. Again, the symbols have their usual meanings.

The first term usually dominates and splits every energy level resulting from the interaction in section 3.1.1 by an amount given by $m_S m_I A$, where $m_S$ and $m_I$ are the magnetic quantum numbers for the electronic and nuclear spins, respectively, and $A$ is given by

$$A = \sqrt{A_{xx}^2 k^2 + A_{yy}^2 \ell^2 + A_{zz}^2 m^2}. \tag{3}$$

In this expression $A_{xx}$, $A_{yy}$ and $A_{zz}$ are the principal values of the hyperfine interaction and $k$, $\ell$ and $m$ are the direction cosines of the magnetic field relative to the principal hyperfine axes.

If $S$ has an integer value then the $2I + 1$ hyperfine levels corresponding to $m_S = 0$ will be nearly degenerate. Under these conditions even small interactions, such as the nuclear Zeeman, quadrupole and higher-order zero-field interactions may scramble the hyperfine levels. Transitions other than those corresponding to $\Delta m_I = 0$ may then have a non-zero transition probability, and instead of the usual three hyperfine lines for a system with $I = 1$,

up to nine transitions are possible. The simple three-line spectrum will, however, still be observed in certain special directions, e.g. if the magnetic field is applied along the main principal axis of the hyperfine interaction. For non-integer electron spin a degeneracy of this nature is not possible for any $m_S$ value. Only minor mixing of the hyperfine levels occurs, and the usual three-line spectrum for nitrogen is likely to be observed for most directions of observation. Since the usual three-line spectrum is the exception rather than the rule, we conclude that $S = 1$ and not $\frac{3}{2}$.

From figures 1 and 3 it follows that there are six and 12 symmetry-related sites for W26 and W25, respectively. To discuss the hyperfine spectra the defects with the specific crystal axes shown in figure 1 will be considered. The $\Delta m_I = 0$ and $\Delta m_I \neq 0$ transitions will be referred to as allowed and forbidden transitions, respectively.

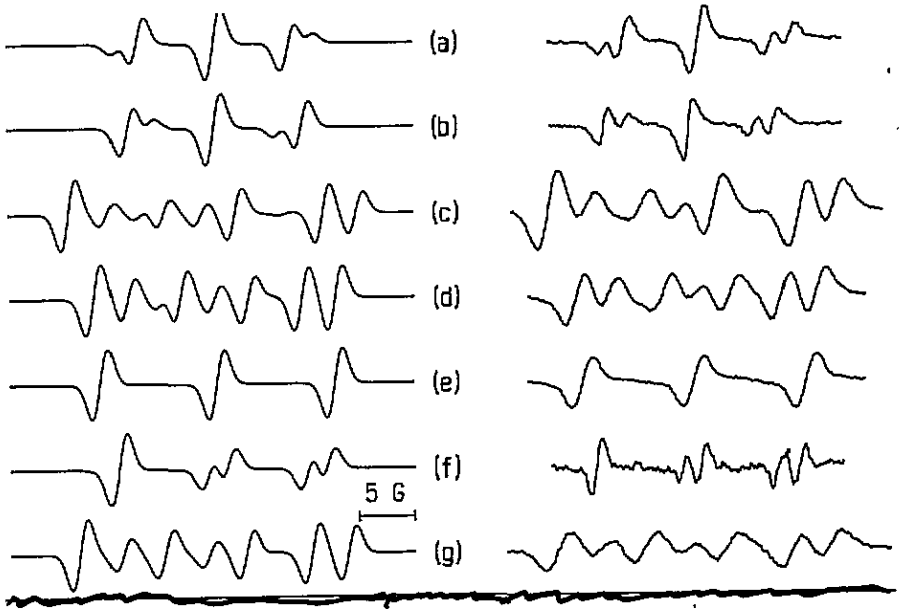


**Figure 4.** Calculated (on the left) and experimental (right) hyperfine spectra for W25. (a) Low field [011]. (b) High field [011]. (c) Low field [01$\bar{1}$]. (d) High field [111]. (e) High field [1$\bar{1}$1]. (f) High field [100]. (g) High field [001].

We turn firstly to the W25 defect. The three-line hyperfine spectrum in figure 4(e), observed when the magnetic field is applied along a ⟨111⟩ direction, shows that the interaction is essentially with one nitrogen and that the main symmetry axis of the hyperfine interaction is probably along, or close to, one of the ⟨111⟩ axes. Further analysis shows that the experimental spectra can be reproduced with a hyperfine interaction which is in fact axially symmetric about a ⟨111⟩ direction lying in the plane perpendicular to the main zero-field axis.

The hyperfine patterns for the [1$\bar{1}$0] and [110] directions (refer to figure 2(b)) differ, and interchange when the symmetry axis of the hyperfine interaction is moved from one of the ⟨111⟩ axes in figure 1(b) to the other while keeping the $x$ axis of the zero-field interaction fixed. Also, the pattern of the lines of spectrum (f) in figure 4 depends on which of the ⟨1$\bar{1}$1⟩ directions is chosen as the main hyperfine axis. The experimental data can be reproduced if the $x$ axis of the zero-field splitting is taken along one of the two ⟨111⟩

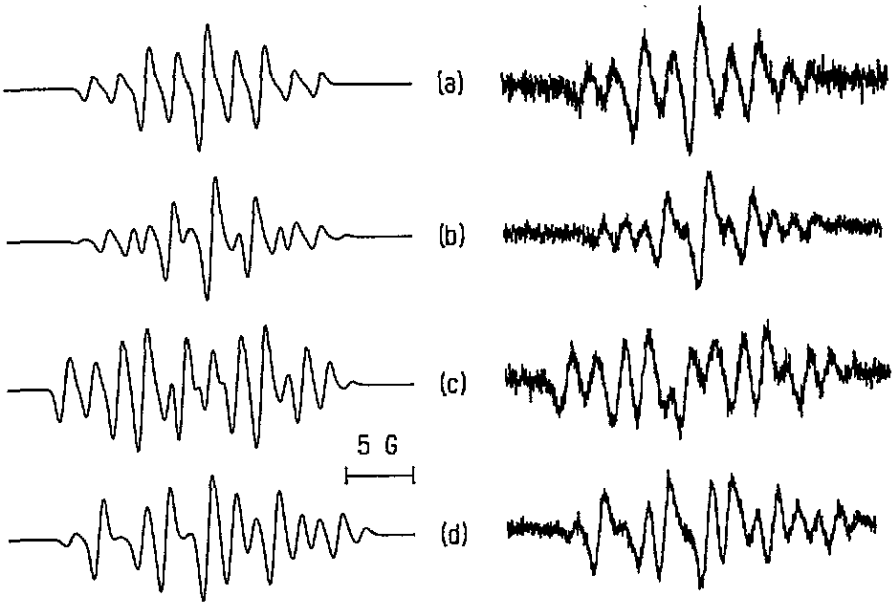


**Figure 5.** Calculated (on the left) and experimental (right) hyperfine spectra for W26. (a) High- and (b) low-field spectra with the magnetic field along [011], i.e. the main symmetry axis of the defect. (c) Low- and (d) high-field spectra with the magnetic field along the [100] direction.

directions and the symmetry axis of the hyperfine interaction along the other. The $x$ axis of the $D$ tensor is therefore along the line joining the two vacancies in figure 1(b). These data are consistent with the model in figure 1(b). The paramagnetic electrons are much closer to the nitrogen on the left, and the hyperfine interaction will be mainly with this nitrogen. Whereas the first-derivative peak to peak linewidths for W26 are around 0.7 G (the value also used for the simulations in figure 5), the linewidths of W25 vary from about 1.2 to about 3 G, depending on the direction in which the spectra are observed. Linewidths used for the simulations in figure 4 were 1.4 G. The hyperfine lines for W25 are therefore noticeably wider than those of W26 and other defects when such are present in the same diamond. A hyperfine coupling of between 1 and 3 MHz, with the more distant nitrogens, can account for the larger linewidths of W25.

The positions and intensities of the forbidden transitions relative to those of the allowed transitions allows the determination of the signs of the interactions relative to each other. If the sign of the hyperfine interaction is changed relative to that of the zero-field interaction, the spectra in figure 4(a) and (b) will also interchange. A comparison of calculated and experimental spectra shows that the hyperfine and zero-field interactions must have opposite signs. The effect of the sign of the quadrupole interaction is best demonstrated by spectrum (f) in figure 4. If this sign is changed the same pattern will be observed except that the high- and low-field components of the spectrum will interchange. This leads to the conclusion that the quadrupole and zero-field interactions must have have the same sign.

Best parameters are given in table 2 and calculated spectra are compared with experimental spectra in figure 4.

An analysis could not be carried out in nearly as much detail for W26. Firstly, note that if the model in figure 1(a) is correct then the paramagnetic electrons will interact with

two identical nitrogens. The hyperfine pattern can then consist of up to $9^2 = 81$ transitions. Referring to figure 1(a), the number of lines is reduced considerably in the $(0\bar{1}1)$ plane, where the nitrogens are equivalent, as in this plane the magnetic field makes equal angles with the axes of the nitrogens. This should also be true in the $[0\bar{1}1]$ direction. In all other directions the nitrogens will be non-equivalent and the intensity of the signal will be divided between many transitions, which is possibly a contributory reason why only a limited number of spectra could be detected for W26.

Reliable hyperfine patterns were detected with the magnetic field along the $z$ and $x$ axes of the defect and are shown in figure 5. These spectra are simulated in figure 5 using the parameters given in tables 1 and 2. The relatively simple spectrum along the $\langle 100 \rangle$ direction shows that the hyperfine pattern due to the two nitrogens will be identical only if one principal axis of the $D$ tensor is also parallel to this direction. This argument justifies the assumption made in the previous section regarding the axes of the $D$ tensor of W26.

Although sufficient spectra were not available to determine unambiguously the relative signs of the parameters, the measured spectra could be reproduced satisfactorily if the signs were chosen as for W25. Also, note that the hyperfine patterns are best reproduced if the hyperfine axes of the nitrogens are tilted towards one another by about 10° from the $\langle 111 \rangle$ directions.

The data, although limited in quantity, are fully consistent with the model in figure 1(a).

**Table 2.** Hyperfine parameters for W25 and W26.

| Parameter | W25 | W26 |
|---|---|---|
| $g_N$ | *0.404* | *0.404* |
| $A_\perp$ (MHz) | 20.6(5) | 10.2(5) |
| $A_\parallel$ (MHz) | 29.4(5) | 21.5(5) |
| $\theta$ (°)[a] | 42(4) | ± 25(3) |
| $P_\parallel$ (MHz) | −4.5(3) | −4.8(3) |
| $\theta$ (°)[a] | 34(4) | ± 25(3) |
| p spin density (%) | 5.3(6) | 6.8(6) |
| s spin density (%) | 1.30(3) | 0.77(3) |
| p/s ratio | 4.1(6) | 9(1) |

[a] $\theta$ is measured from the $\langle 0\bar{1}1 \rangle$ axis in figure 1.

### *3.2. Correspondence of ESR and optical spectra*

The H3 and H4 optical absorption spectra commence growing after a 10 minute anneal at ≈550 °C and begin to saturate in strength after annealing at ≈760 °C. By 800 °C the spectra are fully developed. In figure 6(a) we show the optical spectra, after an anneal at 800 °C, of one of the two specimens that contained only A aggregates (OP2), of two of the three type IaA/B specimens that contain different proportions of A and B aggregates (OP4 and OP5) and one of the two specimens (A35) that contained only B aggregates. In figure 6(b) comparable ESR low-field spectra, with the magnetic field parallel to the $z$ axis, are shown. These spectra should be compared in turn with the corresponding IR spectra (figure 2). In the case of specimen A35, although the H4 optical signal is strong, the ESR spectrum W25 is weak and was difficult to observe. This specimen was however only very weakly luminescent, consistent with the observation mentioned in the introduction that a strong luminescence is a prerequisite for the observation of the ESR signals. It is important, though, to note the complete absence of W26 from the ESR spectrum. The same

observations apply to the other specimen that contained only aggregates (CB7).

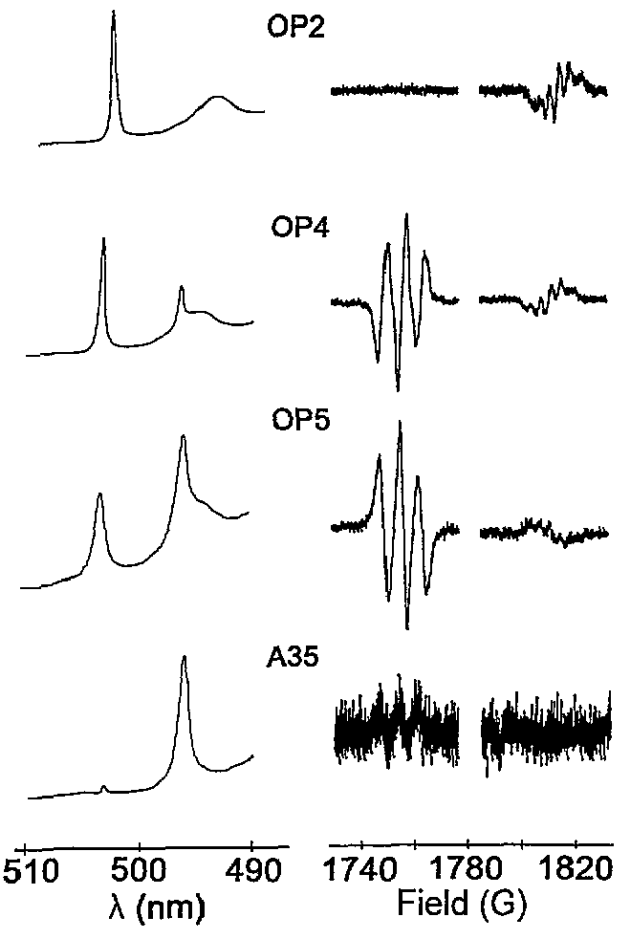


**Figure 6.** A comparison of optical (a) and ESR (b) spectra of several diamonds after annealing for 10 minutes at 800 °C.

## 4. Discussion and conclusions

Comparison of the IR, optical and ESR spectra (section 3.2) shows that in diamonds containing only A aggregates (specimen OP2, and, although not shown, also OP1) only H3 and W26 developed. In specimens containing only B aggregates (A35 and CB7) only H4 and W25 developed. In the mixed-type IaA/B specimens, where A centres and thus H3 dominate (specimen OP4), so too does W26, and when B aggregates become relatively more important (OP5), so too do H4 and W25. There can thus be very little doubt about the identities of W26 and H3, and W25 and H4, respectively.

As with the N–V centre (which will be referred to as W15), which appears in irradiated and annealed type Ib diamonds (Loubser and van Wyk 1977, He *et al* 1993), it is observed that the phases of the high- and low-field lines of W25 and W26 differ when the diamond is exposed to light. In the case of W15 this is because of the preferential population (or

depopulation) of one of the triplet ground state levels (He *et al* 1993). As a consequence of this phenomenon light can enhance the ESR signal by almost two orders of magnitude in some diamonds. W15 is invariably observed in all diamonds in which the optical analogue, a band with zero-phonon line at 637 nm, is present. This does not hold for W25 and W26. The mere presence of the optical absorptions H4 and H3 does not guarantee the observation of the ESR analogues. This shows that the ESR does not arise from the ground states, but from excited states of the defects.

It is accepted (Davies *et al* 1976, Pereira and Monteiro 1991) that the optical spectrum of H3 is due to transitions between $^1A_1$ and $^1B_1$ states. There also exists a vibronically induced $^1A_1$ state 16 meV above the $^1B_1$ state. In order to explain their delayed luminescence data Pereira and Monteiro (1991) proposed the existence of two triplet states about 150 meV below the $^1B_1$ state.

We can arrive at the singlet and triplet states using a very simple model. The similarity between the ESR spectra and optical spectra of H3 and H4 suggests that their spectroscopic characteristics are determined mainly by the electrons in the two dangling bonds. Under $C_{2v}$ symmetry the two molecular orbits formed from the two dangling bonds will transform like $a_1$ and $b_1$. Both electrons in either of these states will give rise to a $^1A_1$ state. One electron in each of the states will result in a $^1B_1$ singlet state and a $^3B_1$ triplet state. The optical transitions then take place between the singlet states and the ESR between the levels of the triplet state. According to Pereira and Monteiro (1991) the lifetime of the electrons in the triplet state must be of the order of tens of milliseconds. It is not clear whether this lifetime is sample dependent, but, if it is, then this may explain why the fluorescence in some diamonds is more intense than in others and why the ESR signals are only observed in these intensely fluorescing diamonds.

The measured zero-field splittings for both defects are surprisingly close to the calculated value expected for two electronic dipoles at next-nearest-neighbour positions in diamond (Lomer and Wild 1973). If the zero-field splittings are indeed dipolar in origin then their signs must be negative. Support for this comes from the fact that the quadrupole and zero-field splittings have the same sign, and the fact that the principal component of the quadrupole interaction has so far been found to be negative for all nitrogen centres in diamond (Cox *et al* 1992, van Wyk and Loubser 1993, Tucker *et al* 1994).

Using the atomic parameters calculated by Morton and Preston (1978), and following Smith *et al* (1959a, b), the p and s spin densities and the p/s ratios have been calculated from the hyperfine parameters. These are included in table 2. The p/s ratio for W25 is comparable to the value for a centre like P2 (van Wyk and Loubser 1993), which also involves a vacancy. For P2 the hyperfine axis is also close to a ⟨111⟩ direction. For W26 the p/s ratio is surprisingly large and is close to the value obtained for the ionized A centre, W24 (van Wyk and Loubser 1983, Tucker *et al* 1994). Also, the hyperfine axes are tilted noticeably towards each other, as if there were a tendency towards the formation of a bond between the two nitrogens.

The electric field gradient, and hence the quadrupole interaction, at a nucleus not only depends on the unpaired electron density, but also on the paired electron densities. Tucker *et al* (1994) considered the contributions of these densities to the field gradient for nitrogen in diamond. It appears that for most nitrogen centres in diamond the principal component of the quadrupole interaction is given by

$$P_{\parallel} = -P_0 f_{2p} + \frac{2P_0\lambda_1^2}{1+\lambda_1^2}\left[1 - |\eta|^2\right] \tag{4}$$

where $P_0$ is the quadrupole interaction parameter for a single electron in a pure $2p_z$ orbital,

$f_{2p}$ and $\lambda_1^2$ are the unpaired electron p spin density and p/s ratio, respectively, and $|\eta|^2$ is the fraction of nitrogen wavefunction involved in each bonding orbital with neighbouring carbon atoms.

The spin densities at the nitrogen nuclei for W25 and W26 should be much like those for the $[N\text{–}V]^{-1}$, also considered by Tucker *et al*, and the equation above ought to apply for these centres. Using $P_0 = -6.7(3)$ MHz (as determined by Tucker *et al*), $|\eta|^2 = 0.5$, relevant data in table 1 and the relation above we find $P_{\|} = -5.0 \pm 1.8$ and $-5.6 \pm 1.5$ MHz for W25 and W26, respectively. Although these values are somewhat larger than the experimental values, they agree within experimental error. Note that the sign of $P_{\|}$ is theoretically predicted to be negative, in agreement with the observation above.

Finally, recent theoretical calculations of the energies (Mainwood 1994), elastic characteristics (Jones *et al* 1994) and vibrational and electronic properties (Jones *et al* 1992) all support the models in figure 1 for H3 and H4.

## Acknowledgments

We should like to thank the management of De Beers Diamond Research Laboratories for providing some of the diamonds used in this work, and to thank also the Diamond Research Laboratories and the Condensed Matter Research Unit of the University of the Witwatersrand for their financial support. We are indebted to Mrs M-L T Rooney (DTC Research Centre, Maidenhead) for her careful work in orienting and polishing specimens.

## References

Clark C D, Ditchburn R W and Dyer H B 1956 *Proc. R. Soc.* A **234** 363
Clark C D and Norris C A 1970 *J. Phys. C: Solid State Phys.* **3** 651
Cox A, Newton M E and Baker J M 1992 *J. Phys.: Condens. Matter* **4** 8119
Davies G 1976 *J. Phys. C: Solid State Phys.* **9** L537
Davies G, Nazaré M H and Hamer M F 1976 *Proc. R. Soc.* A **351** 245
Davies G and Summersgill I 1973 *Diamond Research* p 6
Davies G, Welbourn C M and Loubser J H N 1978 *Diamond Research* p 23
de Sa E S and Davies G 1977 *Proc. R. Soc.* A **357** 231
Elliott R J, Matthews I G and Mitchell E W J 1958 *Phil. Mag.* **3** 360
He X-F, Manson N B and Fisk T H 1993 *Phys. Rev.* **47** 8809
Jones R, Briddon P R and Öberg S 1992 *Phil. Mag. Lett.* **66** 67
Jones R, Torres V J B, Briddon P R and Öberg S 1994 *Proc. 17th Int. Conf. on Defects in Semiconductors (Gmunden, 1993)* ed W Jantsch; *Mater. Sci. Forum* at press
Kaplyanskii A A 1964 *Opt. Spectrosc.* **16** 329
Lomer J N and Wild A M A 1973 *Radiat. Eff.* **17** 37
Loubser J H N and van Wyk J A 1977 *Diamond Research* p 11
——1978 *Rep. Prog. Phys* **41** 1201
——1981 *Diamond Conf. (Reading, 1981)*
Morton J R and Preston K F 1978 *J. Magn. Reson.* **30** 577
Mainwood A 1994 *Phys. Rev.* B **49** 7934
Pereira E and Monteiro T 1991 *J. Lumin.* **48 & 49** 814
Runciman W A 1965 *Proc. Phys. Soc.* **86** 629
Smith W V, Gelles I L and Sorokin P P 1959a *Phys. Rev. Lett.* **2** 39
Smith W V, Sorokin P P, Gelles I L and Lasher G J 1959b *Phys. Rev.* **115** 1546
Tucker O D, Newton M E and Baker J M 1994 *Phys. Rev.* B **50** 15586
van Wyk J A 1982 *J. Phys. C: Solid State Phys.* **15** 981
van Wyk J A and Loubser J H N 1980 *Diamond Conf. (Bristol, 1980)*
——1983 *J. Phys. C: Solid State Phys.* **16** 1501
——1993 *J. Phys.: Condens. Matter* **5** 3019